

Numerical errors of the volume-of-fluid interface tracking algorithm

Gregor Černe¹, Stojan Petelin² and Iztok Tiselj^{1,*},[†]

¹*Reactor Engineering Division, Jožef Stefan Institute, Jamova 39, 1000 Ljubljana, Slovenia*

²*Faculty of Maritime Studies and Transport, University of Ljubljana, 6320 Portorož, Ljubljana, Slovenia*

SUMMARY

One of the important limitations of the interface tracking algorithms is that they can be used only as long as the local computational grid density allows surface tracking. In a dispersed flow, where the dimensions of the particular fluid parts are comparable or smaller than the grid spacing, several numerical and reconstruction errors become considerable. In this paper the analysis of the interface tracking errors is performed for the volume-of-fluid method with the least squares volume of fluid interface reconstruction algorithm. A few simple two-fluid benchmarks are proposed for the investigation of the interface tracking grid dependence. The expression based on the gradient of the volume fraction variable is introduced for the estimation of the reconstruction correctness and can be used for the activation of an adaptive mesh refinement algorithm. Copyright © 2002 John Wiley & Sons, Ltd.

KEY WORDS: interface tracking; interface reconstruction; front capturing; volume of fluid model; adaptive mesh refinement; incompressible multi-fluid flow

1. INTRODUCTION

The interface tracking methods [1] have been widely used for the last 30 years and till now their numerous successful applications proved them to be a very useful tool for the two-fluid flow simulations. Their ability for simulating of the topological changes are usually demonstrated on a small number of typical two-phase flow transients, such as the Rayleigh–Taylor instability [2–8], shape and stability of a rising bubble or falling drop [7, 9–14] just to mention a few. The incessant improvements of these methods and the continuous development of the computer hardware enable more and more complex simulations, such as the free surface motion with automatic mesh generation [15], the 3D simulation of the tens of rising bubbles [16], the merging and fragmentation of the drops [17], precise calculation of the pinching pendant drop [18] and many others.

These successful simulations encouraged also some other applications of the interface tracking algorithms with more complex patterns of the two-fluid flow, e.g. the container filling with

*Correspondence to: I. Tiselj, Reactor Engineering Division, Jožef Stefan Institute, Jamova 39, 1000 Ljubljana, Slovenia.

[†]E-mail: iztok.tiselj@ijs.si

Received November 2000

Revised 14 June 2001

the viscous liquids [19], the dam break flow [20], the falling solid in the gas–liquid system [21], the turbulent mixing of fluids [6], the simulations of some phenomena in the nuclear plants [22], and others. In these simulations the dispersion of the interface occurs and the particular fluid is fragmented into the chunks of the size comparable to the grid size. Since it is obvious that the interface tracking algorithms are limited with the grid size, these examples give rise to a question: is the result a real physical state or is it deformed by the numerical error of the interface tracking algorithm.

Among the variety of interface tracking algorithms we focused on the front capturing methods, more precisely in the volume-of-fluid (VOF) method. The interface reconstruction and calculation of the fluid's motion with the VOF method is largely geometric in nature and it involves some non-physical elements in the simulation. In case the fluid structure is large compared to the grid size these elements are negligible. However, there are numerous two-fluid phenomena, where significant topological change of the interface shape occurs (like the deformation and/or distortion) – in this case the VOF geometrical characteristic might significantly affect the result of the simulation. An example is a phenomenon called a 'numerical surface tension', where the VOF reconstruction algorithm numerically disperses and/or merges the fluid chunks [23]. The simulation on the denser grid can resolve the problem and reduce the influence of the reconstruction incorrectness, however it also increases the computational time.

The main purpose of this paper is to characterize the errors of VOF interface tracking algorithm and to estimate the effect of the grid refinement. It should be noted that similar problems and errors might occur also in other interface tracking algorithms like in front tracking and moving mesh methods. The paper is organized as follows: In Section 2 the main characteristics of the applied VOF model are pointed out, while the third section describes the expression for the reconstruction correctness estimation. In the fourth section we analyse the errors of the VOF interface tracking algorithm and the switch for the grid refinement during the simulations. The last section summarises the main conclusions.

2. THE DESCRIPTION OF THE INTERFACE TRACKING IN THE VOF METHOD

The interface tracking in the VOF method is based on the colour function, which marks the positions of the fluids in the following way [12, 24]

$$f(x, y) = \begin{cases} 1 & \text{if place } (x, y) \text{ is occupied by the fluid 1} \\ 0 & \text{if place } (x, y) \text{ is occupied by the fluid 2} \end{cases} \quad (1)$$

The function f is evaluated on the discrete grid as a volume average:

$$f_{i,j} = \frac{1}{V_{i,j}} \int_{V_{i,j}} f(x, y) dV \quad (2)$$

where $V_{i,j}$ is the volume of the cell (i, j) . The interface tracking in the VOF method consists of the interface reconstruction and of the interface advection algorithm.

2.1. The interface reconstruction algorithm

The interface is reconstructed according to the values of the volume fractions. The algorithm is not unique; there are several with different accuracies and complexities [23–25]. In the present work we used the algorithm based on least squares volume-of-fluid interface reconstruction algorithm (LVIRA) [12, 26] for the reconstruction of the interface. This algorithm makes a linear approximation of the interface by putting a line segment in each multi-fluid cell, i.e., in each cell that has $0 < f_{i,j} < 1$. The approximate interface orientation in the cell (i, j) is determined from the volume fractions in the 3×3 block of the neighbouring cells. The orientation of each interface segment is determined by the normal vector \vec{n} , which is calculated using the gradient of the volume fraction

$$\vec{n} = \frac{\nabla f}{|\nabla f|} = \frac{1}{|\nabla f|} \begin{pmatrix} \frac{1}{3} \sum_{k=-1}^1 f_{i+1,j+k} - f_{i-1,j+k} \\ \frac{1}{3} \sum_{k=-1}^1 f_{i+k,j+1} - f_{i+k,j-1} \end{pmatrix} \quad (3)$$

To improve the convergence of the reconstruction and to make it of second order [26], the orientation \vec{n} is corrected by minimization of the function

$$G_{i,j}(\vec{n}) = \sum_{l=-1}^1 \sum_{k=-1}^1 (f_{i+k,j+l} - f'_{i+k,j+l}(\vec{n}))^2 \quad (4)$$

An example of this algorithm is shown in Figure 1 where fluid 1 and fluid 2 are represented in black and white respectively. The values of $f_{i+k,j+l}$ in Equation (4) are known volume fractions of fluid 1 in the 3×3 block of cells. The values of $f'_{i+k,j+l}(\vec{n})$ are the volume fractions provided by line with the normal \vec{n} and extrapolated on the 3×3 block of cells (dotted line in Figure 1). The line divides the block on the two parts and the volume fractions $f'_{i+k,j+l}(\vec{n})$ are portions of hatched area in the cells. The line is constructed in a way to conserve the volume fraction in the centre cell of the block, i.e., $f_{i,j} = f'_{i,j}$.

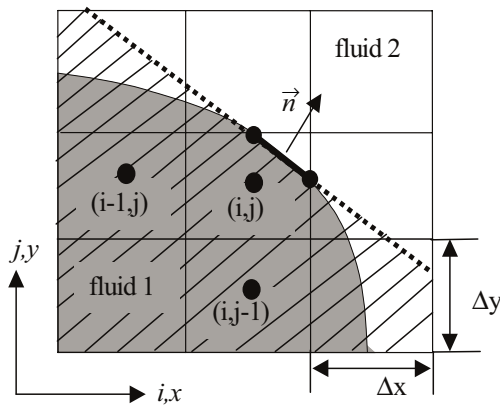


Figure 1. Interface reconstruction with the LVIRA algorithm.

The reconstruction algorithm puts the interface segment between the boundaries of the cell (i, j) (thick black line in Figure 1).

2.2. The interface advection algorithm

The second step in the interface tracking of the VOF method is the advection algorithm, which is used for the time evolution of the volume fractions f . The volume fraction f follows the equation [12, 24]

$$\frac{\partial f}{\partial t} + \nabla \cdot (\vec{u}f) = 0 \quad (5)$$

Equation (5) reflects the fact that in an incompressible fluid the conservation of mass is equivalent to the conservation of volume and hence the conservation of f . Among the several interface advection algorithms [23], we chose an operational split flux procedure [26]. This algorithm may not obey mass conservation exactly, however the integral relative mass error was below $<10^{-4}$ for all the calculations presented in this paper.

The main purpose of the VOF method – of the interface reconstruction and the interface advection algorithm – is to keep the interface sharp during the simulation and to exclude the numerical dispersion of the fluids on the interface.

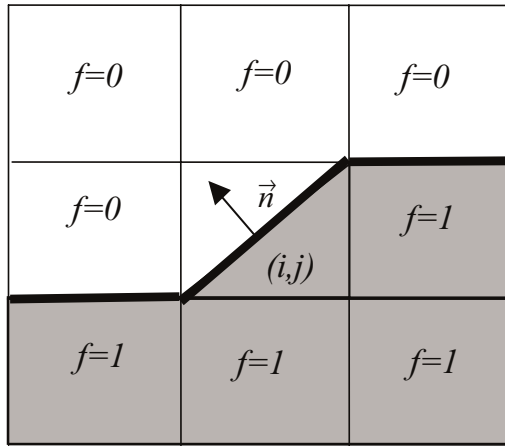
3. THE EXPRESSION FOR THE ‘RECONSTRUCTION CORRECTNESS’

The interface reconstruction and the interface advection algorithms introduce some numerical errors, which might affect the physical properties of the simulation. At the simulation of the general two-fluid flow it is difficult to estimate the numerical errors of the VOF algorithm and their influence on the physical phenomena since the correct solution for the comparison is usually not known. Therefore a numerical expression is needed, which would estimate the reconstruction correctness from the given (calculated) state. Such expression should be based on the volume fraction distribution, since it carries the information about the interface shape. An example of such expression, which is used in the present work, is based on the gradient of volume fraction ∇f

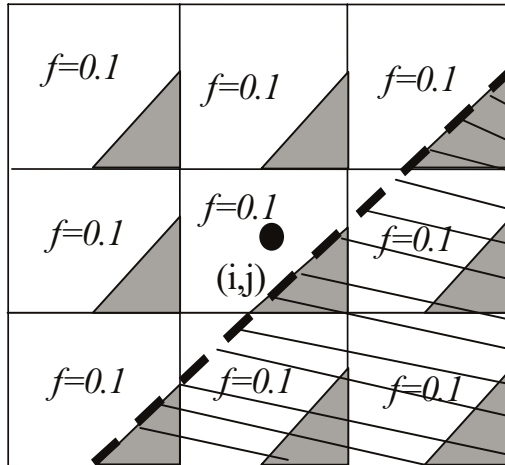
$$\gamma_{i,j} = \sqrt{\left(\frac{1}{3} \sum_{k=-1}^1 f_{i+1,j+k} - f_{i-1,j+k}\right)^2 + \left(\frac{1}{3} \sum_{k=-1}^1 f_{i+k,j+1} - f_{i+k,j-1}\right)^2} \quad (6)$$

The calculation domain of Equation (6) is a 3×3 block of cells. It is used owing to the simple reason – the same area is used for the determination of the interface segment (3) and (4). Before Equation (6) is used for the estimation of the reconstruction correctness its main characteristics have to be analysed. The characteristics like the minimum and the maximum value give some important information about the behaviour of Equation (6). The maximum value of γ can be determined with a short calculation [27] giving $\gamma_{\max} = \sqrt{1 + 1/9} \approx 1.05$. The corresponding state is presented in Figure 2(a).

Equation (6) has the minimum equal to zero in case of homogeneously dispersed fluids $f(x, y) = \text{const}$ (Figure 2(b)), where the gradient of volume fraction is zero. The value of the



(a)



(b)

Figure 2. (a) The maximal value of γ ; (b) the minimal values of γ .

parameter γ is thus close to zero for the dispersed fluids-state where the interface cannot be constructed, and is approaching $\gamma \approx 1$ for clearly separated fluids.

The usage of Equation (6) for reconstruction correctness is not as simple as shown by its maximum and minimum. The only two-fluid state, where the interface is reconstructed on the discrete grid without error are two fluids separated with the linear interface (Figure 3(a)). In that case the values of the reconstruction correctness γ Equation (6) slightly depends on $f_{i,j}$ and relative orientation of the interface to the grid cells ($tg\alpha$ in Figure 3(b)). This dependence is shown in Figure 3(b). The reconstruction correctness γ for the linear interface is between $0.71 \lesssim \gamma \lesssim 1.03$. Of course, an ideal parameter for measuring the dispersion should have a constant value for all positions of the linear interface, however, it is probably impossible to be constructed.

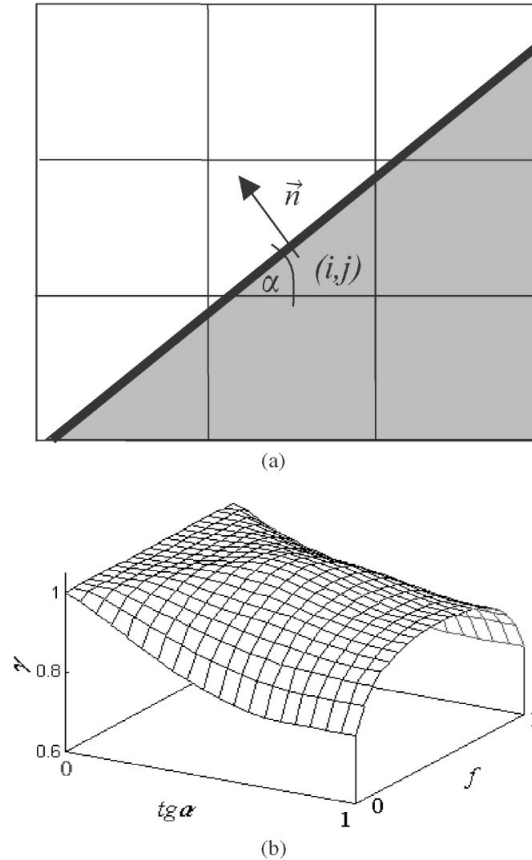


Figure 3. (a) Reconstruction of the linear interface; (b) characteristic of the reconstruction correctness function γ for linear interface.

To reduce the deviation, the reconstruction correctness γ has to be averaged over several cells with the interface. Since the length of the reconstructed interface segment in the cell is not constant (it varies from zero to $h \cdot 2^{1/2}$ where h is the grid size), the averaging should be weighted by the length of the line segments:

$$\bar{\gamma} = \frac{\sum_{i,j} \gamma_{i,j} l_{i,j}}{\sum_{i,j} l_{i,j}} \quad (7)$$

Here $l_{i,j}$ is the length of the interface segment in the cell (i,j) . The summation runs over the mixed cells of the desired area: that is a particular fluid chunk, a part of the interface, or a fixed frame of the cells. The achieved deviation reduction is examined by the calculation of reconstruction correctness $\bar{\gamma}$ on states with its maximal values – fluids separated by the linear interface. The numerical calculation shows that this result varies from $\bar{\gamma} = 1.0$ at $tg\alpha = 0$ to $\bar{\gamma} \cong 0.93$ at $tg\alpha = 1$. The overall average of all possible states with the linear interface gives $\bar{\gamma} \cong 0.97$.

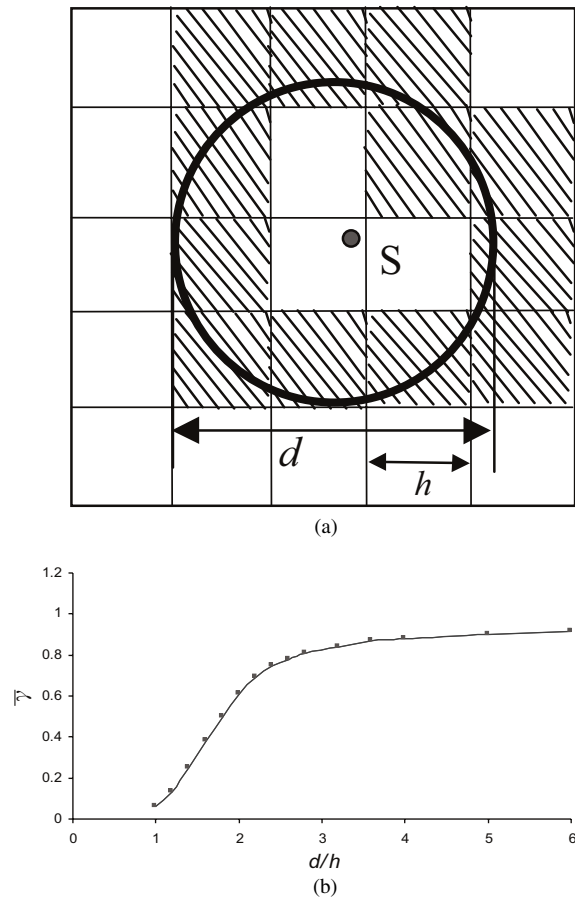


Figure 4. (a) Position of a circular bubble on a grid; (b) reconstruction correctness as a function of the bubble size to grid space ratio.

The proposed reduction of the deviation, Equation (7), is suitable only for the 2D piecewise linear reconstruction, where the length of the reconstructed interface is known. In 3D the area of the reconstructed flat surface piece in the cube cell might be used instead, but its calculation is quite complicated in specific situations. Such a parameter for the reconstruction correctness, which is based on the interface length, also cannot be used in the piecewise constant scheme [28] or stair-step [24] scheme. Other types of averaging should be provided in such cases. The weighted factor should be a function of the gradient ∇f direction and the volume fraction f and having similar characteristic as the length l of the corresponding linear segment.

The application of the reconstruction correctness parameter is simple: if the interface of the specific chunk has the reconstruction correctness close to 1.0, a very small error in the simulation is given by the reconstruction algorithm. Smaller value suggests less reliable simulation by the VOF interface tracking algorithm.

Since the numerical error is larger when smaller chunks are simulated, the reconstruction correctness should have a monotonous dependence on the characteristic chunk size. In order to show this characteristic one of the most common topological shapes in the two-phase flow was used: a bubble. Figure 4(a) shows a circular bubble with the diameter d on a mesh with the grid spacing h . The averaging of the reconstruction correctness $\bar{\gamma}$ is calculated over the whole chunk – in the case shown in Figure 4(a) averaging includes the hatched cells. Parameter $\bar{\gamma}$ as a function of the bubble size (d/h ratio) is shown in Figure 4(b). Larger d/h ratio means more grid cells per bubble and results in larger values of $\bar{\gamma}$. Figure 4(b) shows rapid decrease of $\bar{\gamma}$ values for diameters d less than approximately $3h$. This result is in agreement with the fact, that at least three grid cells per bubble diameter are needed to capture its circular shape with some minimal accuracy, and therefore justifies the choice of $\bar{\gamma}$ as a measure of the interface reconstruction correctness.

4. NUMERICAL EXAMPLES

4.1. The error of the interface reconstruction

The interface reconstruction algorithm causes some error by imitating the curved interface with the line segment. The computed errors are estimated with the L_1 norm defined as

$$\delta = \frac{\sum_{\text{grid}} |f_{i,j}^{\text{calculated}} - f_{i,j}^{\text{exact}}|}{\sum_{\text{grid}} f_{i,j}^{\text{exact}}} \quad (8)$$

The test example for estimating the reconstruction error is a circular 2D bubble. f^{exact} is a volume fraction of the circle calculated on the infinity dense mesh and $f^{\text{calculated}}$ is a volume fraction calculated on some realistic grid. The calculation showed that the L_1 norm (Equation (8)) is calculated within 10 per cent error if f^{exact} is calculated on 16 times denser grid as $f^{\text{calculated}}$. The error (Equation (8)) is smaller when the radius of the curvature is larger. In Figure 5 and Table I we show the reconstruction error (Equation (8)) as a function of the

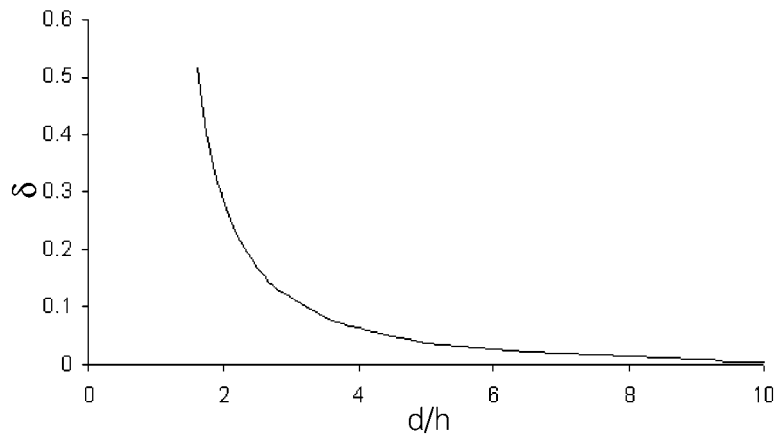


Figure 5. Error of the reconstruction algorithm as a function of the bubble diameter to grid space ratio.

Table I. Reconstruction error of the interface tracking method at different bubble size.

d/h	5	10	20	40	80
error δ	3.8×10^{-2}	5.0×10^{-3}	1.1×10^{-3}	2.3×10^{-4}	4.7×10^{-5}

circle diameter to the grid spacing ratio (d/h). According to these results the relative mass error due to the reconstruction algorithm is less than 10 per cent for the convex chunks with the characteristic size around $d > 3h$.

4.2. The error of the interface advection

The advection error occurs when the fluid chunk moves across the mesh. Figure 6(a) shows a part of the two-fluid state in the two neighbouring cells at the time t . The hatched area is the volume of the specified fluid, which will cross the cell boundary in the next time step $t + \Delta t$. Figure 6(b) shows the state at time $t + \Delta t$ after the advection part of the time step, which preserves the shape of the interface. But in the simulation between the two time steps the LVIRA algorithm reconstructs the interface and changes the interface shape. Figure 6(c) shows the state at the end of the time step when the interface reconstruction substep is finished. The difference of the interface shape between the states in Figure 6(b) and the 6(c) causes the difference of the transferred fluid across the cell boundary and volume fractions in the cells at time $t + 2\Delta t$ ($S_1 \neq S_2$) – so-called advection error.

Figure 7(a) shows the initial state, which consists of several bubbles with different d/h ratios. They are put in the constant velocity field $v(x, y, t) = \text{const}$. The bubbles and fluid around them have the same density and move together as fixed, therefore theoretically the shape of the interface should not change during the transient. Figure 7(b) shows their shape and positions after the time $t = 50h/v$, where v is the prescribed velocity. The effect of the advection error is the deformation of the bubble shape. If the original shape is circular it becomes thicker at the front side after some time. In the case when the chunks are very small

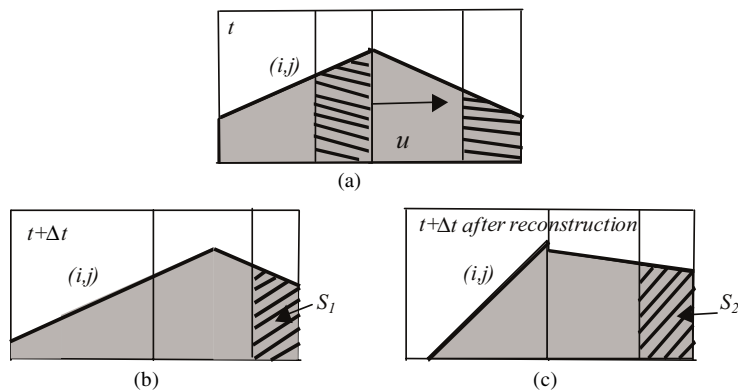


Figure 6. Error of the advection algorithm: (a) the state at time t ; (b) the state of the interface at $t + \Delta t$ after the advection substep; (c) the state at $t + \Delta t$ after the advection and reconstruction substep.

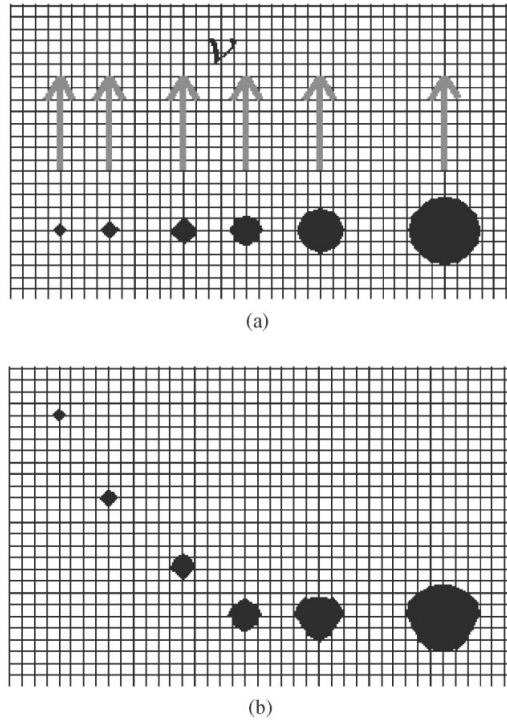


Figure 7. (a) Bubbles in the flow with constant velocity – initial state; (b) bubbles in the flow with constant velocity – state after time $t = 50h/v$.

(characteristic size $d < 2h$), they move faster than the flow field: $v_{\text{chunk}} > v$. Figure 8(a) shows the dependence of the chunk velocity on the circle size d/h . The advection error is calculated similar to Equation (8):

$$\delta = \frac{\sum_{\text{grid}} |f_{i,j}^{t=T} - f_{i,j}^{t=0}|}{\sum_{\text{grid}} f_{i,j}^{t=0}} \quad (9)$$

where $f^{t=0}$ is the volume fraction of the initial state and $f^{t=T}$ is the volume fraction of the final state at $T = 50h/v$. The result in Figure 8(b) shows the advection error δ (Equation (9)) as a function of the characteristic chunk size. The relative volume deformation due to the advection error is below 10 per cent for the chunks with the characteristic sizes around $d > 3.5h$.

4.3. The numerical dispersion

The numerical dispersion occurs when single fluid chunk is reconstructed as several separated pieces due to the numerical errors. One of the simplest cases for the analysis of the numerical dispersion is the deformation of the interface in the shear flow. The velocity field is given by

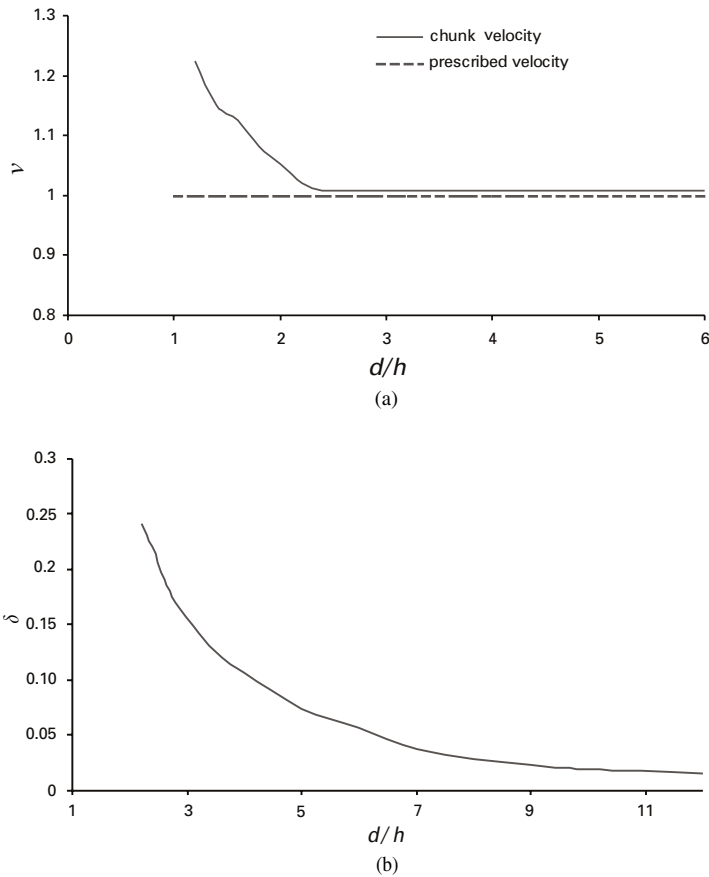


Figure 8. (a) Chunk velocity as a function of the bubble diameter grid space ratio; (b) advection error as a function of the bubble diameter to grid space ratio.

the stream function

$$\Psi = -\frac{1}{2}y^2 \tag{10}$$

where the components of the velocity field in the x and y direction are calculated as $u = -\partial\Psi/\partial y$ and $v = \partial\Psi/\partial x$, respectively.

The initial state of the simulation is a vertical strip – perpendicular to the velocity – with the width d as shown in Figure 9. The applied shear flow stretches the structure to the infinite length, but theoretically it stays continuous. On the other side the numerical simulation is limited by the grid density, which causes the numerical error in the interface reconstruction. Figure 10(a) and (b) shows the state before and after the numerical dispersion occurs. To reduce the computational domain the left and the right boundaries are periodical.

The reconstruction of the linear interface with the VOF method is always correct, which is also valid in the idealized shear flow – no reconstruction and advection errors occur. The numerical dispersion occurs when the thickness of the strip is close to the grid size. In that

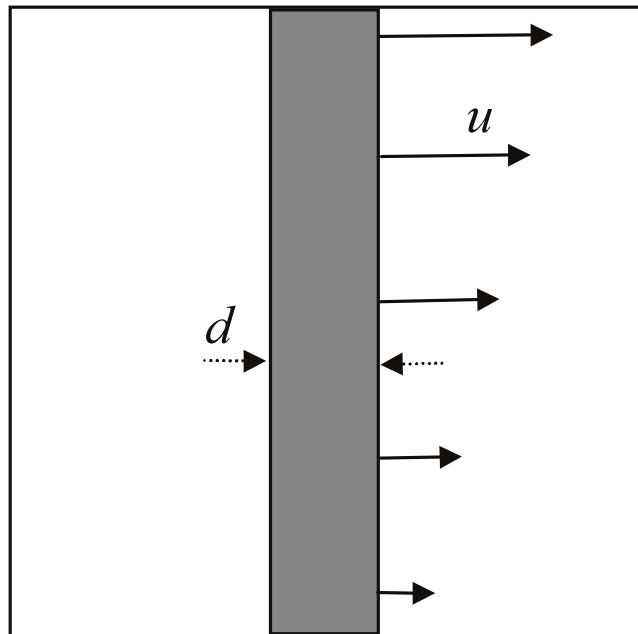


Figure 9. Initial state of the shear flow test.

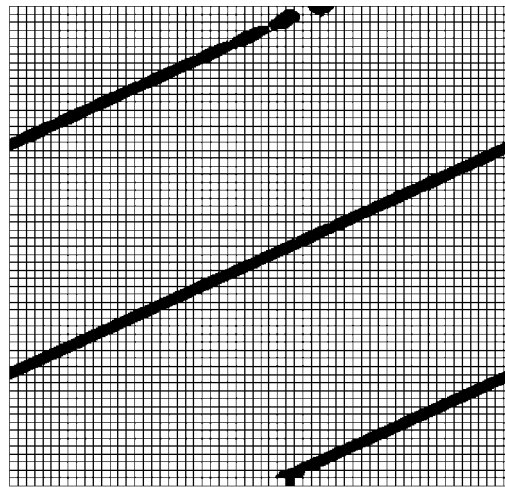
case the gradient of the volume fraction (Equation (3)) does not coincide with the interface normal of the original state and the reconstructed line segment has a wrong orientation. That is seen in Figure 11, where particular line segments are not parallel any more. Different inclination enables the advection error described in Section 4.2 to spoil the result. Parts of the fluid in the mixed cells move faster than the prescribed velocity, and other parts slower. That forms the fluid chunks, which are stable despite the fact that the velocity is not constant across their cross-section. The dotted square in Figure 11 bounds the area, where the numerical chunk is going to form.

The VOF method prevents the dispersion of fluids over the whole area. Instead, it creates a layer of cells where the volume fraction is changing from 1 to 0. The interface reconstruction and interface advection algorithms keep the parts of fluid in the neighbouring cells together. That results in the chunks having characteristic thickness $h < d < 3h$.

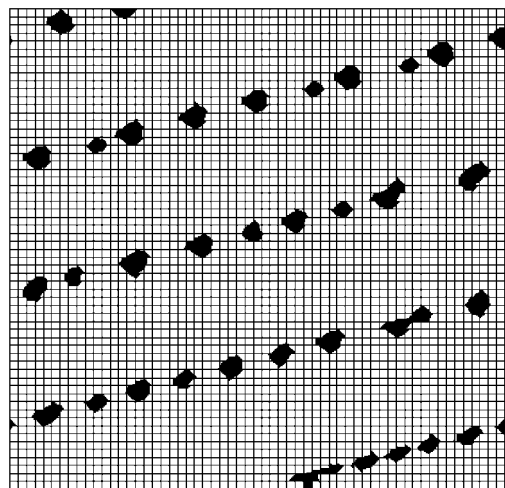
The development of the numerical dispersion can be analysed also using the reconstruction correctness parameter $\bar{\gamma}$ (Equation (6)) calculated for the whole stripe. Its time history is presented in Figure 12. The reconstruction correctness achieves its minimum value when the numerical dispersion occurs (state presented in Figure 10(a)). Later, when the fluid chunks are formed as shown in Figure 10(b), it has approximately constant value, which corresponds to the characteristic size of the fluid chunks.

4.4. The vortical flow

For the overall estimation of the VOF numerical errors, a test problem with the topological changes of the interface is needed. A simple 2D test problem, which is also easy to implement,



(a)



(b)

Figure 10. (a) A vertical stripe deformed by the shear flow before numerical dispersion; (b) a vertical stripe deformed by the shear flow after numerical dispersion.

is vortical flow proposed by Rider and Kothe [23]. Such a test is representative of the interfacial flow in the real physical system like the Rayleigh–Taylor instability where the sharp gradients in the fluid properties lead the transient mechanisms. This test was used in References [23] and [29] for estimating the accuracy of the particular reconstruction algorithms and for the comparison with other reconstructing algorithms. In our case the study is focused on the analysis of the numerical error accumulation and its reduction with the grid refinement.

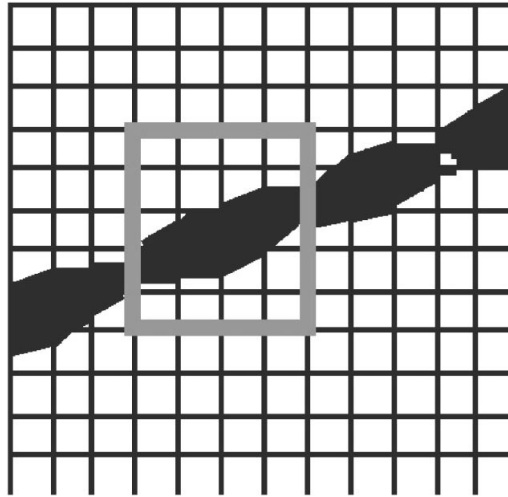


Figure 11. Initiation of the numerical dispersion.

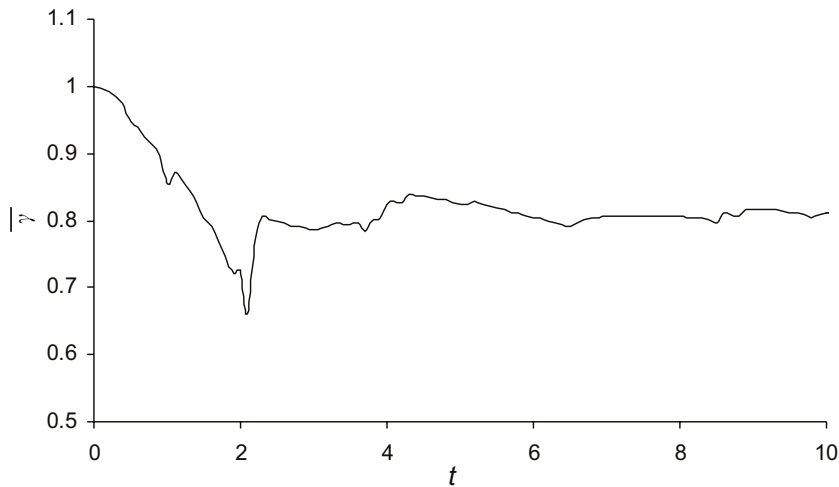


Figure 12. Time history of the reconstruction correctness for the numerical dispersion.

The test uses a fixed velocity field defined by the stream function:

$$\Psi = \frac{1}{\pi} \sin^2(\pi x) \sin^2(\pi y) \cos\left(\pi \frac{t}{T}\right) \quad (11)$$

The initial state is a circle with the radius $r=0.15$, which centre is located in the point $S(0.5,0.8)$ (Figure 13(a)). The vortical velocity defined by Equation (11), which is divergence free, deforms the circle into the spiral as shown in Figure 13(b) for the state at $t=10$ and with $T=50$.

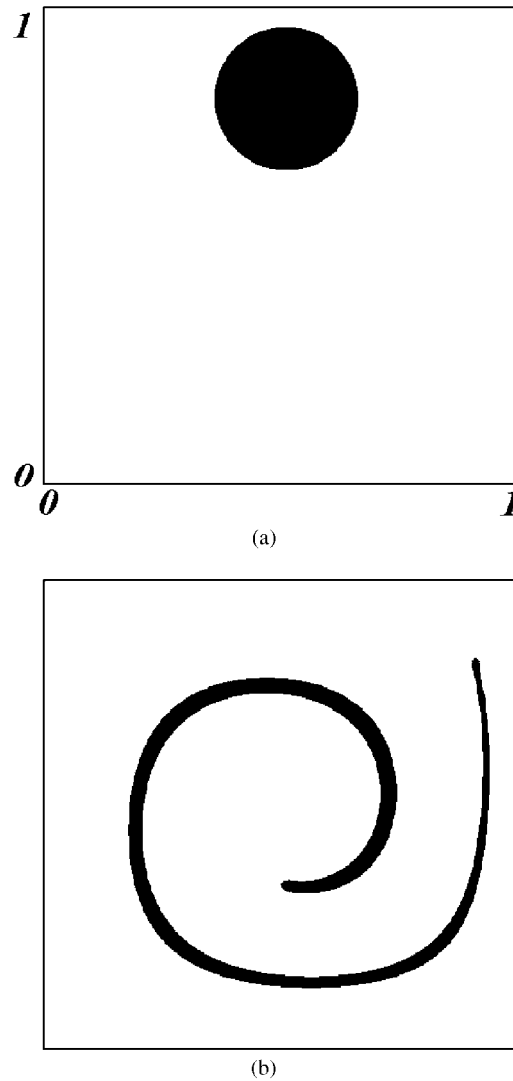


Figure 13. (a) Initial state of the vortex flow; (b) state at $t=10$ and $T=50$.

Theoretically, the fluid structure during the rotation makes a thin stripe and stays continuous even in the case of an infinite whirling T , $t \rightarrow \infty$. During the simulation when the thickness of the fluid is close to the grid size the numerical dispersion occurs (Figure 14). The numerical dispersion is a typical grid dependent phenomenon – a denser grid results in larger number of the dispersed chunks.

After some time at $t=T/2$ the velocity field changes its sign and the fluids are returning back to the initial state at time $t=T$ – but only theoretically. In the simulation the reconstruction and the advection algorithm produce the numerical error, which spoils the result as shown

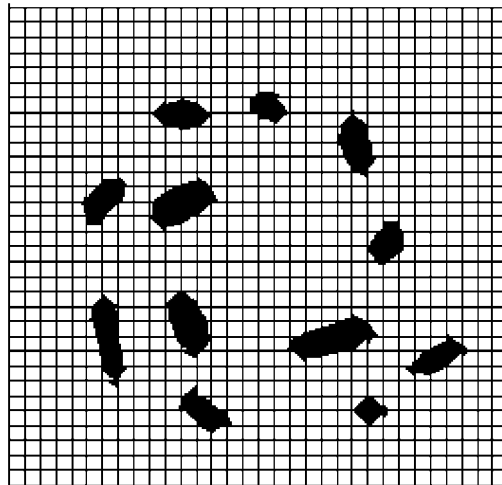
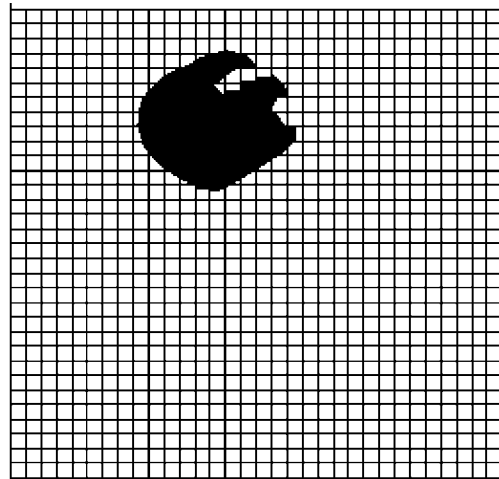


Figure 14. Numerical dispersion on a 30×30 grid.

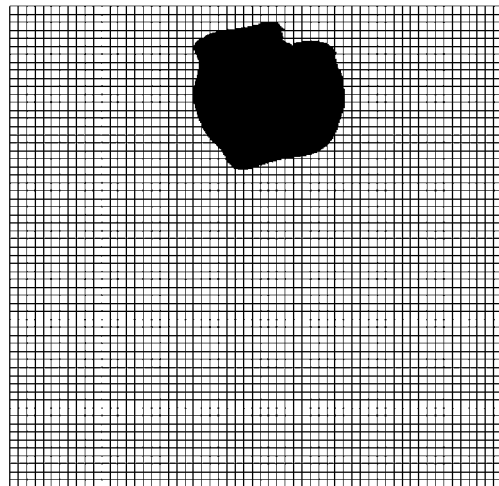
in Figure 15(a) and (b) for two different grid densities. The integral numerical error of the VOF interface tracking algorithm for the transient is calculated with Equation (9) where $f^{t=T}$ and $f^{t=0}$ are the volume fractions of the final and initial state respectively. Figure 16 shows the dependence of the error on the simulation time T . The error δ (Equation (9)) is growing approximately linearly for the times $T < 5$ (vertical dotted line). For the longer transients the error is growing even more rapidly because of the numerical dispersion occurrence.

There are several ways to avoid the numerical interface dispersion, which might have a significant influence on the physical interpretation of the simulation. One way is using a different model, which does not depend so much on the grid density. Such an approach, when the VOF model is replaced by the ‘two-fluid’ model in the moment when the error VOF interface tracking algorithm is apparent, is described in References [8, 30, 31]. The ‘two-fluid’ model is derived by averaging of the basic equations and therefore it is less accurate than the VOF model, but it is capable to give the basic physical picture also on a coarser grid, where the VOF model is defected by numerical errors. Another solution is use of the finer grid, which keeps the accuracy of the VOF interface tracking algorithm. That is seen in Table II, which shows the error δ for vortical flow test at $T=6$ on several grid densities. On the denser grid the error is considerably lower.

The bad side of the calculation on the finer grid is the increase of the computational time and corresponding memory usage. The compromise is to keep the coarse grid as long as the accuracy is still satisfactory and, when not, replace it with finer mesh. This approach is a type of adaptive mesh refinement (AMR). Such a technique has already been used for several times as local AMR in fluid flow simulation [32], or in the interface tracking methods like adhesion of biological cells with the front tracking method [33], the rising bubble with Level set method [34] and adaptive front tracking [35]. In our case a very simple technique of mesh refinement is used. In a moment the state of the whole calculation area is transferred to the double grid density or vice versa. At that moment the velocity field is recalculated according



(a)



(b)

Figure 15. (a) Final state $t=T$ for $T=6$ on 30×30 grid; (b) final state $t=T$ for $T=6$ on 60×60 grid.

to Equation (11) and the volume fractions are transformed geometrically as shown in the Figure 17.

Figure 18(a) shows the error δ as a function of time t_{switch} when the simulation of the swirling flow is switched from 30×30 to the double density 60×60 for the constant $T=6$. The nodalization is switched back to the coarse grid at time $T - t_{\text{switch}}$. The coarse grid does not contribute much to the error at the beginning of the simulation. The simulation, where the switch to double density grid occurs at $t_{\text{switch}} < 1$, has almost the same integral error as in the case when the whole calculation is done on the finer grid. The integral error δ is significantly larger if the switch occurs close to or after the numerical dispersion starts (dotted line in Figure 18(a)).

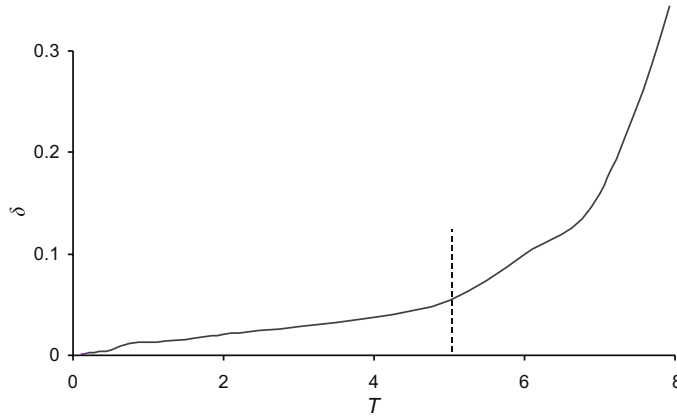
Figure 16. Integral error for the vortical flow on 60×60 grid.

Table II. The grid dependence of the VOF interface tracking error at the vortex flow test.

mesh	15×15	30×30	60×60	120×120
error δ	1.78	0.85	0.098	0.0198

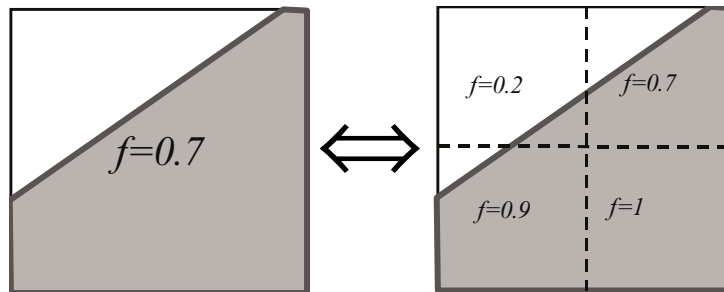


Figure 17. Transformation of the volume fraction to denser/coarser grid.

The grid refinement is more efficient if it is applied before the numerical dispersion occurs. For the estimation when to refine the grid, the reconstruction correctness parameter $\bar{\gamma}$ for the whole fluid chunk is calculated. Finer grid is applied in the moment when $\bar{\gamma} \leq \bar{\gamma}_{\text{switch}}$. In Section 4.3 it is shown that the reconstruction correctness $\bar{\gamma}$ has the minimum value in the moment just before the numerical dispersion occurs. Therefore one can avoid such dispersion by putting $\bar{\gamma}_{\text{switch}}$ equal to or larger than that minimal value $\bar{\gamma}_{\text{switch}} \geq \bar{\gamma}_{\text{min}}$. On the contrary, if $\bar{\gamma}_{\text{switch}} < \bar{\gamma}_{\text{min}}$ the grid refinement has no effect since it never switches on.

The real AMR needs a local criteria for the switch to the double grid density. In general the grid refinement is also more effective when it is carried on locally – on the sub-domain where the local reconstruction correctness is too small. It saves more calculation time and

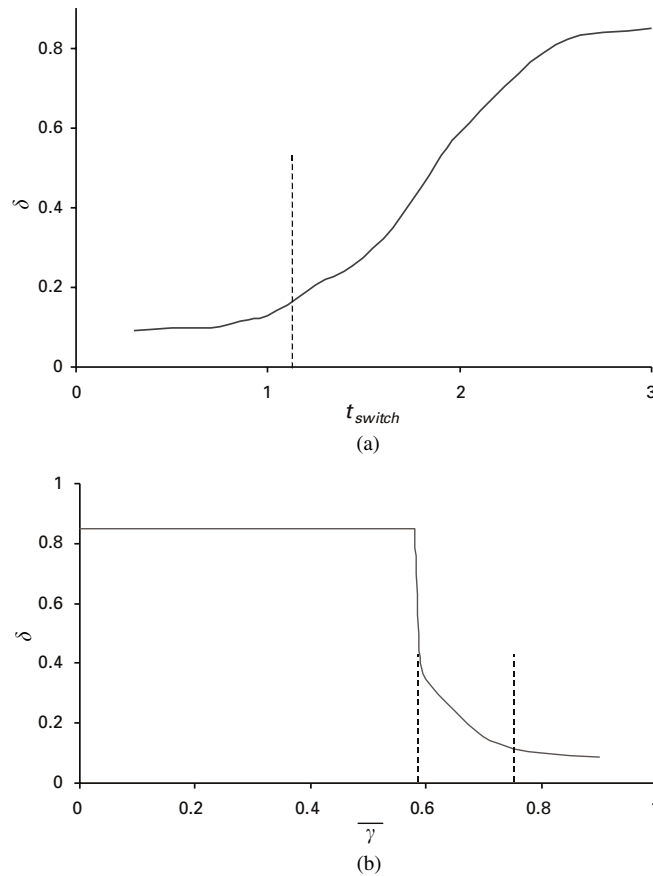


Figure 18. (a) Integral error when the switch to double grid density depends on time; (b) integral error when the switch to double grid density depends on $\bar{\gamma}$.

does not refine the mesh on the place where it is unnecessary. The most suitable way for the calculation of the $\bar{\gamma}$ is the fixed frame of cells, the size of which would be at least a block of 3×3 cells. In our case this is unnecessary, since in the vortical flow the numerical dispersion occurs in a relatively short time interval and the grid refinement is needed on the whole domain. Such simplification saved a lot of programming work and the quality of the grid refinement analysis reminded the same.

Figure 18(b) shows the integral error δ of the VOF interface tracking algorithm, where the switch to double density depends on the $\bar{\gamma}_{switch}$ parameter. The initial grid density is 30×30 . The error is lowered, when the switch to the double density occurs $\bar{\gamma}_{switch} > 0.58$ (the left dotted line in Figure 18(b)). That is the minimal value of the reconstruction correctness, which occurs during this problem. The result in Figure 18(b) shows that the appropriate value for the switch parameter is $\bar{\gamma} > 0.75$. This value keeps the error close to the case simulated exclusively with the double density 60×60 (see Table II). The right dotted line in Figure 18(b) shows the switch to the finest 120×120 grid, which occurs for the $\bar{\gamma}_{switch} > 0.75$ in the present

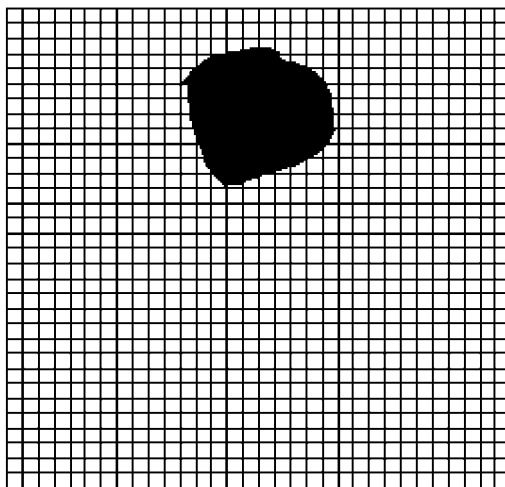


Figure 19. Final state $t=T$ for $T=6$ on 30×30 grid with switch $\gamma_{\text{switch}}=0.8$.

case. The reduction of the error can be noted also in Figure 19, which shows the result at $t=T$ for $T=6$ for the simulation on initial grid 30×30 and switch $\bar{\gamma}_{\text{switch}}=0.8$. This result is much closer to the initial state in Figure 13(a) than the result on pure 30×30 grid in Figure 15(a) and even closer than the result on pure 60×60 grid in Figure 15(b).

Larger value of $\bar{\gamma}_{\text{switch}}$ switches to the double density earlier and makes the integral error δ smaller, however $\bar{\gamma}_{\text{switch}} > 0.9$ does not have a significant effect on it. On the other hand it significantly increases the computational time, since a very dense nodalization is needed to keep the reconstruction correctness so high. The value $\bar{\gamma}_{\text{switch}}$ depends on the need for the accuracy and the calculation time but according to our experience the proposed value should be chosen from the interval $0.75 < \bar{\gamma}_{\text{switch}} < 0.9$.

5. CONCLUSIONS

The simulations with the volume-of fluid model might give some grid-dependent results, which are caused by the errors of the reconstruction and the advection algorithms. Such errors, which might significantly affect the description of the physical phenomena, cannot be avoided by applying better and more accurate front capturing algorithms. The source of this error is the limitation of the grid cell – the VOF model cannot simulate the fluid chunks, which are smaller than the grid cell.

The easiest way for the detection of the numerical error of the VOF model and estimating its influence on the simulation is the comparison to the correct solution. However, that is not possible for the general simulation. The error of the interface tracking is closely connected to the characteristic size of the simulated fluid chunk or the interface part. Therefore a mathematical function is proposed, which has a monotonous dependence on the characteristic size of the fluid chunk, and can serve for the estimation of the numerical error. The gradient of the volume fraction is a kind of the function, which value corresponds to the characteristic size of the fluid chunk and is suitable for the estimation of the VOF interface tracking error.

One possibility for the reduction of the numerical error is the adaptive grid refinement of the mesh during the simulation. The reconstruction correctness function can tell whether the error of the VOF interface tracking algorithm is within the desired accuracy and the coarse grid should be kept, or the denser grid is to be applied.

The test problem with the prescribed velocity proposed in Reference [23] appeared to be very efficient for the study of the reconstruction correctness and evolution of numerical errors on the different grid densities. The study in this paper was performed with the VOF method and the LVIRA piecewise linear reconstruction algorithm, however the results can be applied also for the other VOF reconstruction algorithms.

ACKNOWLEDGEMENTS

The authors are grateful to the Ministry of Education, Science and Sport of the Republic of Slovenia and to Dr Jure Demšar, Jožef Stefan Institute, Slovenia, who has helped to improve the grammar and has made some parts of this paper more understandable.

REFERENCES

1. Hyman LM. Numerical methods for tracking interfaces. *Physica* 1984; **12D**:396–407.
2. Daly JB. Numerical study of two fluid Rayleigh–Taylor instability. *Physics of Fluids* 1967; **10**:297–307.
3. Kelecy FJ, Pletcher RH. The development of a free surface capturing approach for multidimensional free surface flows in closed containers. *Journal of Computational Physics* 1997; **138**:939–980.
4. Mulder W, Osher S, Sethian JA. Computing interface motion in compressible gas dynamics. *Journal of Computational Physics* 1992; **100**:209–228.
5. Unverdi SO, Tryggvason G. Computations of multi-fluid flows. *Physica* 1992; **D60**:70–83.
6. Youngs DL. Numerical simulation of turbulent mixing by Rayleigh–Taylor instability. *Physica* 1984; **D12**:32–44.
7. Pan D, Chang C. The capturing of the free surfaces in incompressible multi-fluid flows. *International Journal for Numerical Methods in Fluids* 2000; **33**:203–222.
8. Černe G, Petelin S, Tiselj I. Coupling of the ‘interface tracking’ and the ‘two-fluid’ models for the simulation of incompressible two-phase flow. *Journal of Computational Physics* 2001; **171**:776–804.
9. Bugg JD, Mack K, Rezkallah KS. A numerical model of Taylor bubbles rising through stagnant liquids in vertical tubes. *International Journal of Multiphase Flow* 1998; **24**(2):271–281.
10. Chen L, Garimella SV, Reizes JA, Leonardi E. The development of a bubble rising in a viscous liquid. *Journal of Fluid Mechanics* 1999; **387**:61–96.
11. Han J, Tryggvason G. Secondary breakup of axisymmetric liquid drops. I. Acceleration by a constant body force. *Physics of Fluids* 1999; **11**:3650–3666.
12. Puckett EG, Almgren AS, Bell JB, Marcus DL, Rider WJ. A high order projection method for tracking fluid interfaces in variable density incompressible flows. *Journal of Computational Physics* 1997; **130**:269–282.
13. Sussman M, Smereka P, Osher S. A level set approach for computing solutions to incompressible two-phase flow. *Journal of Computational Physics* 1994; **114**:146–159.
14. Unverdi SO, Tryggvason G. A front-tracking method for viscous, incompressible, multi-fluid flows. *Journal of Computational Physics* 1992; **100**:25–37.
15. Peterson RC, Jimack PK, Kelmanson MA. The solution of two-dimensional free-surface problems using automatic mesh generation. *International Journal for Numerical Methods in Fluids* 1999; **31**:937–960.
16. Bunner B, Tryggvason G. Direct numerical simulation of three-dimensional bubbly flows. *Physics of Fluids (Letters)* 1999; **11**(8):1967–1969.
17. Lafaurie B, Nardone C, Scardovelli R, Zaleski S, Zanetti G. Modelling merging and fragmentation in multiphase flows with SURFER. *Journal of Computational Physics* 1994; **113**:134–147.
18. Gueyffier D, Li J, Nadim A, Scardovelli R, Zaleski S. Volume-of-fluid interface tracking with smoothed surface stress methods for three-dimensional flows. *Journal of Computational Physics* 1999; **152**:423–456.
19. Tome MF, Mckee S, Barratt L, Jarvis DA, Patrick AJ. An experimental and numerical investigation of container filling with viscous liquids. *International Journal for Numerical Methods in Fluids* 1999; **31**:1333–1353.
20. Brufau P, Garcia-Navarro P. Two-dimensional dam break flow simulation. *International Journal for Numerical Methods in Fluids* 2000; **33**:35–57.

21. Minato A, Takamori K, Ishida N. Numerical method for interaction between gas–liquid two-phase flow and solid motion. *Two-Phase Flow Modelling and Experimentation*, 1999; 1537–1543.
22. Ohashi H. Advanced numerical simulation for complex flow phenomena. *Eighth International Topical Meeting on Nuclear Reactor Thermal-Hydraulics. Proceedings*, 1997; vol. 1: 461–467.
23. Rider WJ, Kothe DB. Reconstructing volume tracking. *Journal of Computational Physics* 1998; **141**:112–152.
24. Hirt CW, Nichols BD. Volume of fluid (VOF) method for the dynamics of free boundaries. *Journal of Computational Physics* 1981; **39**:201–225.
25. Ashgriz N, Poo JY. Flair: Flux line segment model for advection and interface reconstruction. *Journal of Computational Physics* 1991; **93**:449–468.
26. Zaleski S. Volume of fluid (VOF) methods. Short Courses. *Modelling and Computation of Multiphase Flows*, Part: IIB ‘Multiphase-Flow CFD’. Zurich, Switzerland, 1999.
27. Černe G. Two-fluid flow simulation with coupling of volume-of-fluid model and two-fluid model. Thesis, University of Ljubljana, Ljubljana, 2001.
28. Noh WF, Woodward PR. SLIC (simple line interface calculation). *Proceedings, Fifth International Conference on Fluid Dynamics. Lecture Notes in Physics*. Springer: Berlin, 1976; **59**:330–340.
29. Ubbink O, Issa RI. A method for capturing sharp fluid interfaces on arbitrary meshes. *Journal of Computational Physics* 1999; **153**:26–50.
30. Černe G, Petelin S. Numerical simulation of transition from stratified to slug flow in a horizontal pipe. *ZAMM*. 2000; **153**:S715–S716.
31. Černe G, Petelin S, Tiselj I. Simulation of the instability in the stratified two-fluid system. *Proceedings of Nuclear Energy in Central Europe’99*, 1999; 201–208.
32. Papadakis G, Bergeles G. A local grid refinement method for three-dimensional turbulent recirculating flows. *International Journal for Numerical Methods in Fluids* 1999; **31**:1157–1172.
33. Agresar G, Linderman JJ, Tryggvason G, Powell KG. An adaptive, cartesian, front-tracking method for the motion, deformation and adhesion of circulating cells. *Journal of Computational Physics* 1998; **143**:346–380.
34. Sussman M, Almgren AS, Bell JB, Colella P, Howell LH, Welcome M. An adaptive level set approach for incompressible two-phase flows. *Proceedings of the ASME Fluids Engineering Summer Meeting: Forum on Advances in Numerical Modeling of Free Surface and Interface Dynamics*, 1996, vol. 3: p. 355.
35. Galaktionov OS, Anderson PD, Peters GWM, Van de Vosse FN. An adaptive front tracking technique for three-dimensional transient flows. *International Journal for Numerical Methods in Fluids* 2000; **32**:201–217.